

Cosmic microwave background observations: implications for Hubble's constant and the spectral parameters n and Q in cold dark matter critical density universes

Charles H. Lineweaver¹ and Domingos Barbosa^{1,2}

¹ Observatoire astronomique de Strasbourg, U.L.P., F-67000 Strasbourg, France.

² Centro de Astrofísica da U.P., Rua do Campo Alegre 823, PT-4150 Porto, Portugal.

Received 2 December 1996 / Accepted 21 May 1997

Abstract. Recent cosmic microwave background (CMB) measurements over a large range of angular scales have become sensitive enough to provide interesting constraints on cosmological parameters within a restricted class of models. We use the CMB measurements to study inflation-based, cold dark matter (CDM) critical density universes. We explore the 4-dimensional parameter space having as free parameters, Hubble's constant H_o , baryonic fraction Ω_b , the spectral slope of scalar perturbations n and the power spectrum quadrupole normalization Q . We calculate χ^2 minimization values and likelihood intervals for these parameters. Within the models considered, a low value for the Hubble constant is preferred: $H_o = 30^{+18}_{-7}$ km s⁻¹Mpc⁻¹. The baryonic fraction is not as well-constrained by the CMB data: $\Omega_b = 0.07^{+0.24}_{-0.07}$. The power spectrum slope is $n = 0.91^{+0.20}_{-0.12}$. The power spectrum normalization is $Q = 18 \pm 2.5 \mu\text{K}$. The error bars on each parameter are approximately 1σ and are for the case where the other 3 parameters have been marginalized. If we condition on $n = 1$ we obtain the normalization $Q = 17 \pm 1.0 \mu\text{K}$. The permitted regions of the 4-D parameter space are presented in a series of 2-D projections. In the context of the CDM critical density universes considered here, current CMB data favor a low value for the Hubble constant. Such low- H_o models are consistent with Big Bang nucleosynthesis, cluster baryonic fractions, the large-scale distribution of galaxies and the ages of globular clusters; although in disagreement with direct determinations of the Hubble constant.

Key words: cosmic microwave background – cosmology: observations – theory

1. Introduction

The standard picture of structure formation relies on the gravitational amplification of initially small perturbations in the

matter distribution. The origin of these fluctuations is unclear, but a popular assumption is that these fluctuations originate in the very early universe during an inflationary epoch. The most straightforward incarnation of this inflationary scenario predicts that the fluctuations are adiabatic, Gaussian, Harrison-Zeldovich ($n = 1$) and that the Universe is spatially flat (Kolb & Turner 1990). To avoid violating primordial nucleosynthesis constraints, the Universe should be dominated by non-baryonic matter. The cold dark matter (CDM) model has been the preferred model in the inflationary scenario (Peebles 1982, Liddle and Lyth, 1993).

The statistical properties of CMB fluctuations provide an ideal tool for testing CDM models. CMB data offer valuable information not only on the scenario of the origin of cosmic structures, but also on the early physics of the Universe and the cosmological parameters that characterize the Universe. Using the CMB to determine these parameters is the beginning of a new era in cosmology. This truly cosmological method probes scales much larger and epochs much earlier ($z > 1000$) than more traditional techniques which rely on supernovae, galaxies, galaxy clusters and other low-redshift objects. The CMB probes the entire observable universe.

Acoustic oscillations of the baryon–photon fluid at recombination produce peaks and valleys in the CMB power spectrum at sub-degree angular scales. Measurements of these model-dependent peaks and valleys have the potential to determine many important cosmological parameters to the few percent level (Jungman et al. 1996, Zaldarriaga et al. 1997). Within the next decade, increasingly accurate sub-degree scale CMB observations from the ground, from balloons and particularly from two new satellites (MAP: Wright et al. 1996, Planck Surveyor: Bersanelli et al. 1996) will tell us the ultimate fate of the Universe (Ω_o), what the Universe is made of (Ω_b , Ω_{CDM}) and the age and size of the Universe ($h \equiv H_o/(100/\text{km s}^{-1}\text{Mpc}^{-1})$) with unprecedented precision.

In preparation for the increasingly fruitful harvests of data, it is important to determine what the combined CMB data can *already* tell us about the cosmological parameters. In Lineweaver

Send offprint requests to: Charley Lineweaver,
charley@edwin.phys.unsw.edu.au

et al. (1997), (henceforth “paper I”), we compared the most recent CMB data to predictions of COBE normalized flat universes with Harrison-Zel’dovich ($n = 1$) power spectra. We used predominantly goodness-of-fit statistics to locate the regions of parameter space preferred by the CMB data. We explored the $h - \Omega_b$ plane and the $h - \lambda_o$ plane.

In the present paper we focus on the range for h favored by the CMB in the context of CDM critical density universes and we broaden the scope of our exploration to the 4-dimensional parameter space: h , Ω_b , n and Q . Our motivation for choosing this 4-D subspace of the higher dimensional parameter space is that (i) it is the largest dimensional subspace that we can explore at a reasonable resolution with the means available and (ii) it is centered on the simplest CDM model: $\Omega_o = 1$, $\lambda_o = 0$, $n = 1$. This model is arguably the simplest scenario for the formation of large-scale structure. One of our goals is to see what is required of such a model if it is to explain the current set of large-scale structure data, and what could eventually force us to accept the fine-tuning demanded by the inclusion of another cosmological parameter, such as the cosmological constant.

Hubble’s constant H_o is possibly the most important parameter in cosmology, giving the expansion rate, age and size of the Universe. Recent, direct, low-redshift measurements fall in the range [45-90] but may be subject to unidentified systematic errors. Thus it is important to have different methods which may not be subject to the same systematics. For example, CMB determinations of h are distance-ladder-independent. Current CMB data are not of high enough quality to draw definitive model-independent conclusions, however in the restricted class of models considered here, the CMB data are already able to provide interesting constraints.

The quantity Ω_b is important because we would like to know what the Universe is made of and how much normal baryonic matter exists in it. The combination $\Omega_b h^2$ is relatively well-constrained by the observations and theory of primordial nucleosynthesis, but the uncertainty on the Hubble constant means that the value of Ω_b is rather poorly constrained. The question of just how many baryons there are in the Universe has received close attention recently due to estimates of the baryon fraction in galaxy clusters and attempts to constrain Ω_b by measuring the deuterium in high-redshift quasar absorption systems.

The parameter n is the primordial power spectrum slope that remains equal to its primordial value at the largest scales (low ℓ). It is important because it’s measurement is a glimpse at the primordial universe. Although generic inflation predicts $n = 1$, a larger set of plausible inflationary models is consistent with $0.7 \lesssim n \lesssim 1.0$. Model power spectra and particularly the amplitude of the first peak depend strongly on n . Thus, an important limitation of paper I was the restriction to $n = 1$. By adding n as a free parameter we obtain observational limits on n and quantify the reduced constraining ability of the CMB observations when n is marginalized.

The power spectrum quadrupole normalization Q is important because it normalizes all models. Here we treat Q as a free parameter.

We examine how the constraints on any one of these parameters change as we condition on and marginalize over the other parameters. We obtain χ^2 minimization values and likelihood intervals for h , Ω_b , n and Q . As in paper I, we take advantage of the recently available fast Boltzmann code (Seljak & Zaldarriga 1996) to make a detailed exploration of parameter space.

All the results reported here were obtained under a restrictive set of assumptions. We assume inflation-based CDM models of structure formation with Gaussian adiabatic initial conditions in critical density universes ($\Omega_o = 1$) with no cosmological constant ($\lambda_o = 0$). We have ignored the possibility of early reionization and any gravity wave contribution to the spectra. We do not test topological defect models. We use no hot dark matter. We have used the helium fraction $Y_{He} = 0.24$ and a mean CMB temperature $T_o = 2.728$ K. Although we have not yet looked carefully at how dependent our results are on these assumptions we make some informed estimates in Sect. 6.1 where we also discuss previous work using similar data sets and similar methods to look at different families of models.

In Sect. 2 we describe the data analysis. In Sect. 3 we present our results for h and Ω_b and discuss their dependence on some plausible variations in the data analysis. We discuss non-CMB constraints and compare them with our results in Sect. 4. In Sect. 5 we present our results for n and Q . In Sect. 6 we add some caveats and summarize.

2. Method

2.1. Data

The data used are described in paper I, however we have updated some data points and now include several more measurements:

- updated Tenerife point (Hancock et al. 1997): $\delta T_{eff} = 34.1^{+15.5}_{-9.3}$ at $\ell_{eff} = 20$,
- added BAM point (Tucker et al. 1997): $\delta T_{eff} = 55.6^{+29.6}_{-15.2}$ at $\ell_{eff} = 74$,
- updated the two Python points (Platt et al. 1997): $\delta T_{eff} = 60^{+15}_{-13}$ at $\ell_{eff} = 87$ and $\delta T_{eff} = 66^{+17}_{-16}$ at $\ell_{eff} = 170$,
- added MSAM single- and double-difference points (Cheng et al. 1996) $\delta T_{eff} = 40.7^{+30.5}_{-17.0}$ at $\ell_{eff} = 159$ $\delta T_{eff} = 44.4^{+23.9}_{-14.5}$ at $\ell_{eff} = 263$.

With the exception of the Saskatoon points, the calibration uncertainties of the experiments were added in quadrature to the error bars on the points. The MSAM values are the weighted averages of the first and second MSAM flights. The error bars assigned encompass the 1σ limits from both flights. In paper I, we did not include the MSAM points because of possible correlations with the Saskatoon results. However the MSAM results are substantially lower than the Saskatoon results in this crucial high- ℓ region of the power spectrum and it is not clear that avoiding such correlations is more important than the additional information provided by the MSAM data. The figures presented in this paper include the MSAM points however we have also performed χ^2 calculations without MSAM. We discuss these results in Sect. 3.1.

2.2. Calculation

A two-dimensional version of our χ^2 calculation is described in paper I. In this work we generalize to 5 dimensions and use a likelihood approach to determine the parameter ranges. We treat the correlated calibration uncertainty of the 5 Saskatoon points as a nuisance parameter “ u ”. For each point in 5-D space we obtain a value for $\chi^2(h, \Omega_b, n, Q, u)$. We assume u comes from a Gaussian distribution about its nominal value with a dispersion of 14%. This Gaussian assumption amounts to adding $[(1-u)/0.14]^2$ to the χ^2 calculation described in paper I. For example, in paper I, our notation Sk-14, Sk0 and Sk+14 corresponds to $u = (0.86, 1.00, 1.14)$ respectively (however we did not assume a Gaussian distribution and so did not add the extra factor to the χ^2 values).

For each point in the 4-D space of interesting parameters, u takes on the value which minimizes the χ^2 (Avni 1976, Wright 1994). At the minimum in 4-D, χ^2_{min} , the parameter values are the best-fit parameters. To obtain error bars on these values, we determine the 4-D surfaces which satisfy $\chi^2(h, \Omega_b, n, Q) = \chi^2_{min} + x$ where $x = [1, 4, 9, 16]$. Under the assumption that the errors on the data points are Gaussian (cf. de Bernardis et al. 1997), the $x = 1$ ellipsoid can be projected onto any of the axes to get the 1σ confidence interval for the parameter of that axis. If one is not interested in 1-D intervals but rather in the confidence regions for 2 parameters simultaneously, then one would use $x = [2.3, 6.17, 11.8, 19.3]$ (see Press et al. 1989 for details). To make the figures, we project the 4-D surfaces onto the two dimensions of our choice and obtain contours which we project onto either axis.

We have normalized the power spectra using the conversion $C_\ell = Q^2 \frac{4\pi}{5} \frac{C'_\ell}{C^2_\ell}$, where C'_ℓ is the power spectrum output of the Boltzmann code.

3. Results for h and Ω_b

The permitted regions of the 4-D parameter space are presented in a series of 2-D projections which contain likelihood contours from a combination of the most recent CMB measurements. There are four groups of figures corresponding to the four planes $h - \Omega_b$, $h - n$, $h - Q$ and $n - Q$; Figs. 1–3, 5, 6–7 and 8–9 respectively. The thick ‘X’ in each figure marks the minimum. Areas within the 1σ contours have been shaded.

The best-fit values and confidence intervals displayed in the figures are summarized in Table 1 which thus contains the main results of this work. The values of h , Ω_b , n and Q at the minimum of the 4-D χ^2 are given with error bars from the projection onto 1-D of the $\chi^2_{min} + 1$ surface. In Figs. 1 through 4 the region preferred by Big Bang nucleosynthesis (BBN) is shaded light grey ($0.010 < \Omega_b h^2 < 0.026$, see Sect. 4.1).

In Fig. 1 we have conditioned on $n = 1$ and $Q = 17 \mu\text{K}$. The results are $h = 0.35^{+0.08}_{-0.05}$, $\Omega_b = 0.02^{+0.04}_{-0.02}$. At 2σ , $0.25 < h < 0.60$ and $0.0 < \Omega_b < 0.13$.

The contours and notation of Fig. 2 are the same as in Fig. 1 except that we have let the normalization Q be a free parameter. That is, for each value of h and Ω_b , Q takes on the value (within

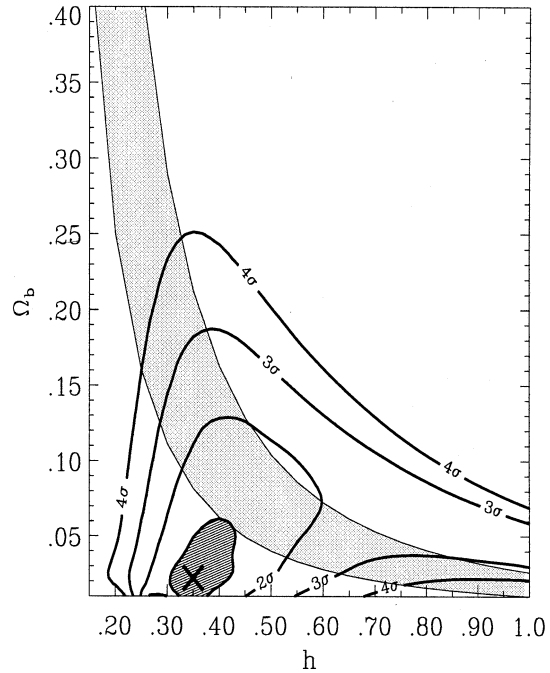


Fig. 1. Likelihood contours in the $h - \Omega_b$ plane from recent CMB measurements. We have conditioned on $n = 1$ and $Q = 17 \mu\text{K}$. The ‘X’ marks the minimum. The contours are at levels $\chi^2_{min} + x$ where $x = [1, 4, 9, 16]$ (see Sect. 2.2). When projected onto either of the axes these regions give the approximate size of the 1, 2, 3 and 4σ confidence intervals respectively. The area within the 1σ contour has been shaded dark grey. The result, $h = 0.35^{+0.08}_{-0.05}$, $\Omega_b = 0.02^{+0.04}_{-0.02}$, is given in Table 1. Big Bang nucleosynthesis predictions favor the light grey band defined by $0.010 < \Omega_b h^2 < 0.026$ (see Sect. 4.1).

the discretely sampled range) which minimizes $\chi^2(h, \Omega_b)$. The minimum and the 1σ errors on h and Ω_b are the same as in Fig. 1; h stays low. The 2, 3, and 4σ contours are noticeably larger than in Fig. 1. Within the 2σ contours, the higher values of Ω_b permitted correspond to $Q < 17 \mu\text{K}$.

Fig. 3 displays the main result for h of this paper. The result is more general than the results of Figs. 1 and 2 since no restrictions on n and Q are used. Examining Figs. 1, 2 and 3 sequentially, the dark grey 1σ contours can be seen to get larger as we first condition on and then marginalize over n and Q . With both n and Q marginalized we obtain $h = 0.30^{+0.18}_{-0.06}$ and $\Omega_b = 0.07^{+0.24}_{-0.07}$ where the error bars are approximately 1σ . At the minimum, $n = 0.91$ and $Q = 18 \mu\text{K}$. The χ^2 value at this minimum is 16. The number of degrees of freedom is 23 (= 27 data points – 1 nuisance parameter – 3 marginalized parameters). The probability of finding a χ^2 value this low or lower is $\sim 15\%$. Thus the fit obtained is “good”.

The region of the $h - \Omega_b$ plane acceptable to both the BBN and CMB have low values of h . Large values of h , especially in the BBN region (lower right of plot) are not favored by the CMB data. However at 2σ , h is unconstrained since the projection of the 2σ contours onto the h axis spans the entire axis.

Since n is a free parameter the amplitude, but not the location, of the Doppler peak can vary substantially. This explains

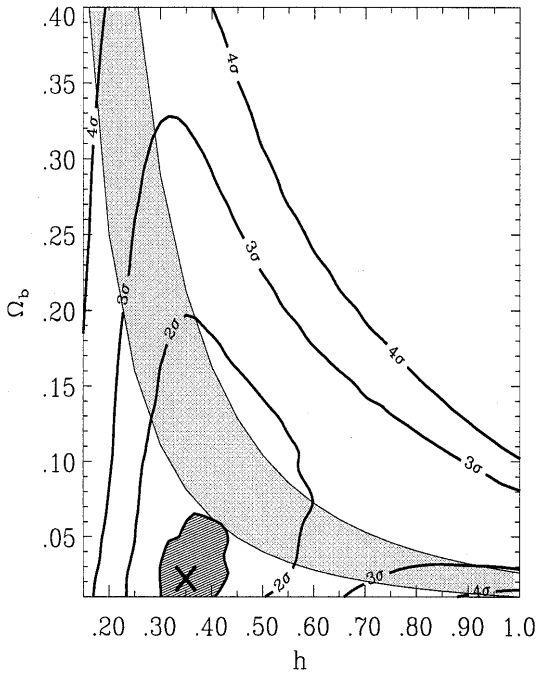


Fig. 2. Contours and notation as in previous figure except here the normalization Q has become a free parameter, i.e., for a given h and Ω_b , Q takes on the value that minimizes the value of χ^2 at that point. The minimum and the 1σ errors on h and Ω_b are the same as in Fig. 1 however the 2, 3, and 4σ contours are noticeably larger. The higher values of Ω_b permitted here correspond to $Q < 17 \mu\text{K}$.

the shape of the 68% region allowed by the data: the possible range of Ω_b is enlarged, but not the confidence interval of the Hubble constant, which seems to be predominantly determined by the position of the Doppler peak.

The disjoint 2σ contour region on the right is characterized by the parameter values $h \gtrsim 0.65$, $\Omega_b \sim 0.15$, $n \approx 0.7 \pm 0.1$ and $Q \approx 20 \pm 2 \mu\text{K}$. The minimum χ^2 of this region is at $h = 1.0$.

3.1. Robustness of results to data analysis choices

Since there is a $\sim 2\sigma$ inconsistency between the MSAM and the Saskatoon data and since there may be unknown systematic errors, we have performed some checks to see how dependent our results are on the various ways of analyzing the data.

• Without MSAM

The figures and Table 1 results include the MSAM data points, but we have also performed χ^2 calculations without the MSAM data points. When the MSAM points are not included the h and Ω_b minimum and contours do not change significantly. For example the results from Fig. 3 without MSAM are $h = 0.30^{+0.18}_{-0.08}$ and $\Omega_b = 0.08^{+0.24}_{-0.08}$.

• Saskatoon calibration treatment

We have treated the Saskatoon calibration as a nuisance parameter from a Gaussian distribution around the nominal Saskatoon calibration with a dispersion of 14%. The values of u at the minimum χ^2 in this technique are $u \sim 0.82$. Netterfield et al. (1997) have compared the Saskatoon results to the MSAM first flight

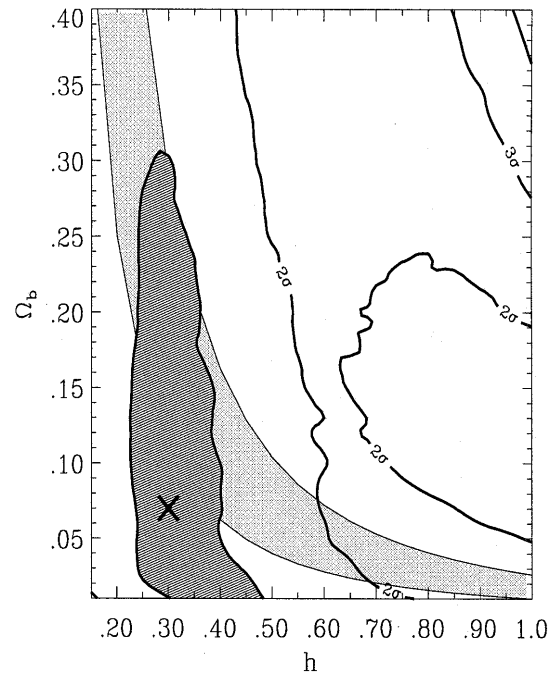


Fig. 3. Same as previous figure except here both Q and n are free parameters. The preferred value of h stays low: $h = 0.30^{+0.18}_{-0.07}$ but at 2σ , h can assume all values tested, i.e., the projection of the 2σ region onto the h axis covers the entire axis. We also find $\Omega_b = 0.07^{+0.24}_{-0.07}$. At the minimum $n = 0.91$ and $Q = 18 \mu\text{K}$. In contrast to the previous figure the higher values of Ω_b permitted correspond to $Q > 17 \mu\text{K}$ and $n < 1$. On the right, the high h , $\Omega_b \sim 0.15$ region within the 2σ contour has $n \sim 0.7$ and $Q \sim 20 \mu\text{K}$.

results in the north polar region observed by both experiments. They find a best-fit calibration of -18% which is equivalent to the 0.82 discussed above. Thus, there is some evidence for a lower nominal Saskatoon calibration.

However, preliminary results based on a relative calibration between Jupiter and Cas A at 32 GHz imply that a $+5\% \pm 7\%$ Saskatoon calibration is appropriate (Leitch et al. 1997). Using this calibration changes the results slightly. For example, the analog of Fig. 3 yields tighter contours around the unchanged h minimum: $h = 0.30^{+0.10}_{-0.07}$ and $\Omega_b = 0.19$ with 1σ error bars larger than the range probed. The preference for $\Omega_b \sim 0.15-0.20$ is increased (independent of h) and the avoidance of the high h , low Ω_b , BBN region is increased. The χ^2 value of the minimum increases from ≈ 16 to ≈ 21 thus the fit is still good; 42% probability of having a lower χ^2 .

We have also let u be a free parameter from a uniform distribution, i.e., a free-floating Saskatoon calibration. The analog of Fig. 3 yields $h = 0.30^{+0.23}_{-0.07}$, $\Omega_b = 0.05^{+0.20}_{-0.05}$. At the minimum $u = 0.78$ ($= -22\%$), $\chi^2 = 14$ and the probability of obtaining a lower χ^2 is 7%. We have also obtained results assuming three different Saskatoon calibrations; the nominal value, 14% higher and 14% lower. The minimum χ^2 stays at $h \approx 0.30$ in all three cases.

Thus several plausible choices of data selection and data analysis producing $\sim 20\%$ variations in the amplitude of the

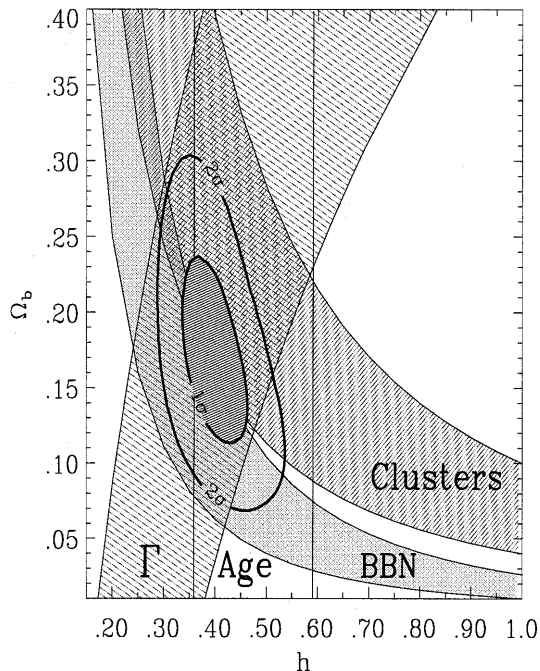


Fig. 4. This plot has no CMB information in it. The bands are the constraints from 4 non-CMB measurements discussed in Sect. 4: Big Bang nucleosynthesis (“BBN”), cluster baryonic fraction (“Clusters”), the galaxy and cluster scale density fluctuation shape parameter (“ Γ ”) and the age of the oldest stars in globular clusters (“Age”: region between the vertical lines). To quantify the combination of these 4 constraints, we show contours obtained by assuming for each constraint a two-tailed Gaussian probability around the central values. The 1 and 2 σ contours are thus the result of an approximate joint likelihood of 4 non-CMB constraints for $\Omega_o = 1$, $\lambda_o = 0$ CDM models. A low h is preferred. This was pointed out in Bartlett et al. (1995). The combination of these four, independent, non-CMB measurements yields $H_o \approx 40 \pm 7$ and $\Omega_b \approx 0.18 \pm 0.06$. This region of the $h - \Omega_b$ plane is very similar to the region preferred by the CMB data (compare Fig. 3). The point of this diagram is *not* to show that h is low since we have ignored the numerous, more direct, $z \sim 0$ measurements of h which find $h \approx 0.70 \pm 0.10$. The point of this diagram is to show that an important set of independent constraints also favors low values of h in $\Omega_o = 1$, $\lambda_o = 0$ CDM models.

Doppler peak, do not strongly affect the low h results from the CMB. The many measurements on the Doppler slope in the interval $[10 < \ell < 200]$ contribute strongly to determining the position of the peak and thus to the preference for low h (see Figs. 3 and 4 of paper I). $h \approx 0.30$ appears to be a fairly robust CMB result for the critical density CDM models tested here.

3.2. Ω_b results

Our CMB constraints on Ω_b are weaker than our constraints on h ; the 1 σ contours in Fig. 3 are elongated vertically and yield $\Omega_b = 0.07^{+0.24}_{-0.07}$. Comparing Figs. 1 and 2 with 3, one sees that it is the marginalization over n which opens the $\Omega_b \gtrsim 0.07$ region (where $n < 0.9$). White et al. (1996) highlight the merits of high baryonic fraction ($\Omega_b \sim 10\% - 15\%$) models. We confirm

Table 1. parameter results

Results ^a	Conditions			
	h	$\Omega_b(\%)$	n	Q(μ K)
$H_o =$	35^{+8}_{-5}	free ^b	1	17
	35^{+8}_{-5}	free	1	free
	30^{+18}_{-7}	free	free	free
	$^{c}40^{+7}_{-7}$	—	—	—
$\Omega_b(\%) =$	2^{+4}_{-2}	free	1	17
	2^{+4}_{-2}	free	1	free
	7^{+24}_{-7}	free	free	free
	$^{c}18^{+6}_{-6}$	—	—	—
n =	$1.03^{+0.07}_{-0.06}$	0.50	5	free
	$0.91^{+0.20}_{-0.12}$	free	free	free
Q(μ K) =	$17^{+1.0}_{-1.0}$	free	free	1
	$17^{+1.5}_{-2.0}$	0.50	5	free
	$18^{+2.5}_{-2.5}$	free	free	free

^a parameter values at the χ^2 minimum. The error bars come from the projected 1 σ contours in the figures.

^b “free” means that the parameters were free to take on any value within the discretely sampled range which minimized the value of χ^2 . As a result of the discretization, these reported minima can be displaced from the true minima by up to half a grid point on both axes, i.e., $H_o = 30$ should be taken to mean, $27.5 \leq H_o \leq 32.5$. The underlying matrix of model points is described by $0.15 \leq h \leq 1.00$, step size: 0.05, $0.01 \leq \Omega_b \leq 0.4$, step size: 0.012, $0.5 \leq n \leq 1.5$, step size: 0.06, $10 \leq Q \leq 30$, step size: 1. Thus we have tested over 200,000 ($18 \times 34 \times 18 \times 20$) models.

^c Result from joint likelihood of non-CMB constraints (see Fig. 4).

that the CMB χ^2 1 σ region is centered near this range but the valley of minima is very shallow. In the context of our models, non-CMB data can still constrain Ω_b slightly better than the CMB. See our discussion of Fig. 4 in Sect. 4.5 where we report $\Omega_b \approx 0.18 \pm 0.06$.

4. Non-CMB constraints in the $h - \Omega_b$ plane

Four independent non-CMB cosmological measurements constrain the acceptable regions of the $h - \Omega_b$ plane.

4.1. Nucleosynthesis

Primordial nucleosynthesis gives us limits on the baryonic density of the Universe. Although deuterium measurements seem to be currently the most accurate baryometer, there is an active debate about whether they yield high (Tytler et al. 1996, Tytler & Burles 1997) or low (Songaila et al. 1994, Carswell et al. 1994, Rugers & Hogan 1996) baryonic densities. We have adopted the range $0.010 < \Omega_b h^2 < 0.026$ because it encompasses most published results. These limits are plotted in Figs. 1 - 4 and are labelled “BBN” in Fig. 4. We use $\Omega_b = 0.015$ as a central value. The BBN constraints are independent of Ω_o , λ_o , n and Q and thus do not depend on our $\Omega_o = 1$, $\lambda_o = 0$ assumptions. Lyman limit systems yield a somewhat model-dependent lower limit for the baryonic density, lending support to the higher values of $\Omega_b h^2$ (Weinberg et al. 1997, Bi & Davidsen 1997).

4.2. X-ray cluster baryonic mass fraction

Observations of the X-ray luminosity and the angular size of galaxy clusters can be combined to constrain the quantity $\frac{\Omega_b}{\Omega_o} h^{3/2}$. We adopt the range $0.04 < \frac{\Omega_b}{\Omega_o} h^{3/2} < 0.10$ (White et al. 1993) with a central value of 0.06 (Evrard 1997). These limits seem to be inconsistent with BBN if $\Omega_o = 1$ and $h \gtrsim 0.50$. This is known as the baryon catastrophe and has led some to believe that $\Omega_o < 1$. The severity of this catastrophe in $\Omega_o = 1$ models can be examined in Fig. 4 by comparing the “BBN” region with the “Clusters” region. For $\Omega_b \gtrsim 0.15$, $\Omega_o = 1$ models allow consistency between the nucleosynthetic and cluster data for low values of h .

4.3. Matter power spectrum shape parameter Γ

Peacock & Dodds (1994) made an empirical fit to the matter power spectrum using a shape parameter Γ . For $\Omega_o \leq 1$ models, Γ can be written as (Sugiyama 1995)

$$\Gamma = h \Omega_o \exp \left[-\Omega_b \left(\frac{\Omega_o + 1}{\Omega_o} \right) \right]. \quad (1)$$

We adopt the 2σ limits of the empirical fit of Peacock & Dodds (1994) (see also Liddle et al. 1996a) and include the n dependence

$$0.222 < \Gamma - 0.32 \left(\frac{1}{n} - 1 \right) < 0.293. \quad (2)$$

Under the assumption that $0.8 \leq n \leq 1.2$, Eq. 2 becomes $0.169 \leq \Gamma \leq 0.373$. This is the Γ constraint used in Fig. 4. We use $\Gamma = 0.25$ as a central value.

4.4. Limits on the age of the Universe from the oldest stars in globular clusters

There is general agreement that the Universe should be older than the oldest stars in our Galaxy. Thus a lower bound on the age of the Universe comes from an age determination of the oldest stars in the most metal-poor (= oldest) globular clusters. A reasonably representative sample of globular cluster ages, t_{gc} , in the literature is,

Bolte & Hogan (1995)	13.7	$< t_{gc} <$	17.9
Sarajedini et al. (1995)	13.7	$< t_{gc} <$	14.3
Chaboyer (1995)	11	$< t_{gc} <$	21
Jimenez et al. (1996)	11.5	$< t_{gc} <$	15.5
Salaris et al. (1997)	10.4	$< t_{gc} <$	14.0

Allowing ~ 1 Gyr for the formation of globular clusters, we adopt the range $11 < t_o < 18$ Gyr with a central value of 14 Gyr. We use this relatively large interval to avoid overconstraining the models and to encompass most published results. Age determinations are Ω_o and λ_o independent but converting them to limits on Hubble’s parameter depends on our $\Omega_o = 1$ and $\lambda_o = 0$ assumptions. In the models we are considering here, our age limits are converted directly into limits on Hubble’s constant using $h = 6.52 \text{ Gyr}/t_o$ which yields $0.59 > h > 0.36$ (with the central value 14 Gyr corresponding to $h = 0.47$). This region is marked “Age” in Fig. 4.

4.5. Summary of non-CMB constraints and comparison to CMB constraints

The constraints we adopt from BBN, cluster baryonic fraction, Γ , and the ages of the oldest stars in globular clusters (as described above) are,

BBN	0.010	$<$	$\Omega_b h^2$	$<$	0.026
Clusters	0.04	$<$	$\Omega_b h^{3/2}$	$<$	0.10
Γ	0.169	$<$	Γ	$<$	0.373
GC Ages	0.36	$<$	h	$<$	0.59

Bands illustrating these constraints are plotted in Fig. 4. Since these constraints are independent, it is not obvious that they should be consistent with each other. They are consistent in the sense that there is a region of overlap. This consistency is improved if $\Omega_b h^2$ turns out to be high as indicated by Tytler & Burles (1997). To visualize more quantitatively the combination of these four constraints, for each constraint we assume a two-tailed Gaussian distribution around the central values. This allows the flexibility to account for asymmetric error bars. We then calculate a joint likelihood,

$$\mathcal{L}(h, \Omega_b) = \mathcal{L}_{BBN} * \mathcal{L}_{clus} * \mathcal{L}_{\Gamma} * \mathcal{L}_{age} \quad (3)$$

where,

$$\mathcal{L}_{BBN}(h, \Omega_b) \propto \exp \left[-\frac{(\Omega_b h^2 - 0.015)^2}{2 \sigma_{BBN}^2} \right] \quad (4)$$

$$\mathcal{L}_{clus}(h, \Omega_b) \propto \exp \left[-\frac{(\Omega_b h^{3/2} - 0.06)^2}{2 \sigma_{clus}^2} \right] \quad (5)$$

$$\mathcal{L}_{\Gamma}(h, \Omega_b) \propto \exp \left[-\frac{(\Gamma(h, \Omega_b) - 0.25)^2}{2 \sigma_{\Gamma}^2} \right] \quad (6)$$

$$\mathcal{L}_{age}(h) \propto \exp \left[-\frac{(h - 0.47)^2}{2 \sigma_{age}^2} \right] \quad (7)$$

$$(8)$$

The upper and lower limits of the four constraints determine the σ ’s for the two-tailed Gaussians. For example $\sigma_{BBN,up} = (0.026 - 0.015)$ and $\sigma_{BBN,down} = (0.015 - 0.010)$. The joint likelihood of the four terms $\mathcal{L}_{BBN} * \mathcal{L}_{clus} * \mathcal{L}_{\Gamma} * \mathcal{L}_{age}$ is shown in Fig. 4. The contour levels are $\mathcal{L}(h, \Omega_b)/\mathcal{L}_{max} = \exp(-\frac{1}{2}[1, 4])$. The combined non-CMB constraints from BBN, cluster baryonic fraction, Γ and stellar ages yield $h \approx 0.40 \pm 0.07$ and $\Omega_b \approx 0.18 \pm 0.06$ for $\Omega_o = 1$, $\lambda_o = 0$.

The point of Fig. 4 is *not* to show that h is low since we have of course ignored the numerous, more direct, $z \sim 0$ measurements of h which find $h \approx 0.70 \pm 0.10$ (see for example Freedman 1997). The point of this diagram is to show that an important set of independent constraints do overlap and are consistent with each other for low values of h in the $\Omega_o = 1$, $\lambda_o = 0$ models considered here.

Fig. 4 should be compared with Fig. 3 which has contours of $\mathcal{L}_{CMB}(h, \Omega_b) \propto \exp \left[-\frac{\chi^2(h, \Omega_b)}{2} \right]$. There is an interesting consistency between the non-CMB constraints and the CMB constraints of Fig. 3. Although they extend over relatively small

regions in the $h - \Omega_b$ plane, the 1σ regions of the non-CMB joint likelihood and the CMB overlap.

In Fig. 4 we see that the combination of four independent cosmological measurements indicate that a low value of h could make the CDM theory viable, as Bartlett et al. (1995) argued. The amplitude of small scale matter fluctuations is an additional consistency check on this model. The value of σ_8 at the minimum in Fig. 3 is $\sigma_8 = 0.54$. This agrees quite well with values inferred from X-ray cluster data (Viana & Liddle 1996, Oukbir et al. 1996).

Liddle et al. (1996b) studied critical density CDM models. Based on the COBE normalization, peculiar velocity flows, the galaxy correlation function, abundances of galaxy clusters, quasars and damped Lyman alpha systems, they found that $h < 0.50$ and $n < 1$ is preferred. Adams et al. (1997) come to similar conclusions.

Bartlett et al. (1995) listed the advantages of a low h in critical density universes, the main point being that there exists a region of parameter space in which this simplest of models remains consistent with observations of the large-scale structure of the Universe. For example, there is the question of the age crisis. Recent h measurements point to values in the interval $0.60 < h < 0.80$. In a critical density universe $h = 0.70$ implies an age of 9.3 Gyr, younger than the estimated age of many globular clusters. $h = 0.30$ yields an age for the universe of 21.7 Gyr comfortably in accord with globular cluster ages.

What is perhaps surprising is the fact that the CMB data do not rule out such a low value of H_0 but seem to favor it within the context of this type of scenario. Of course, these low H_0 values are in disagreement with current measurements of the Hubble constant.

4.6. Other projections

Figs. 5 through 9 show our 4-D χ^2 ellipsoid projected on to 2-D planes orthogonal to the $h - \Omega_b$ plane. The limits obtained on h from Fig. 5 are the same as we obtained from Fig. 3 since we are projecting the same 4-D χ^2 surface. h and n are positively correlated for $h \lesssim 0.50$ and possibly negatively correlated for $h \gtrsim 0.50$. In Fig. 6 we see that with n fixed at 1, a high precision determination of Q is possible, $Q = 17 \pm 1.0 \mu\text{K}$. In Fig. 7 the $n = 1$ constraint is dropped.

5. Results for n and Q

Figs. 8 and 9 show the strong anti-correlation between n and Q . This has been observed and discussed by many authors (e.g. Smoot et al. 1992, Seljak & Bertschinger 1993, Lineweaver 1994). This anti-correlation has a simple explanation. In the $C_\ell(\ell)$ plot, any increase of the slope lowers the y-intercept (at $\ell = 2$) and any decrease of the slope raises the y-intercept. The anti-correlation is thus inherent with the use of the amplitude at $\ell = 2$ as the normalization.

The increase of the size of the error bars on n and Q as h and Ω_b are conditioned on and then marginalized can be seen by comparing Figs. 8 and 9. Our n and Q results are $n = 0.91^{+0.20}_{-0.12}$

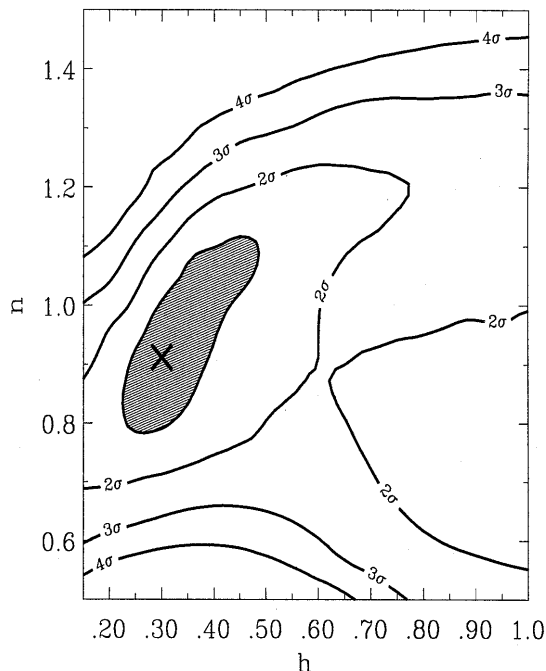


Fig. 5. Likelihood contours in the $h - n$ plane for Ω_b free and Q free. $h = 0.30^{+0.18}_{-0.07}$ and $n = 0.91^{+0.20}_{-0.12}$. The $h \gtrsim 0.80$ region has $Q \sim 20 \mu\text{K}$. At 2σ , $0.55 < n < 1.23$, and the largest n is for $0.50 < h < 0.70$. In the 1σ contour there is a strong h and n correlation: the lower values of h go with the lower values of n . When different values of n are allowed, the amplitude of the Doppler peak varies up and down but the location of the peak does not.

and $Q = 18 \pm 2.5 \mu\text{K}$ from Fig. 9 where both h and Ω_b have been marginalized. Conditioning on $n = 1$, we get $Q = 17 \pm 1.0 \mu\text{K}$ (see also Fig. 6).

The four year COBE-DMR constraints on the amplitude and slope of the power spectrum at large angular scales are $n_{DMR} = 1.2 \pm 0.3$ and $Q = 15.3^{+3.8}_{-2.8} \mu\text{K}$, and conditioning on $n_{DMR} = 1$, $Q = 18 \pm 1.6 \mu\text{K}$ (Bennett et al. 1996). These DMR results are in the context of $\Omega_o = 1$, $\lambda_o = 0$ CDM models and they need to be corrected due to the mildly model-dependent extended tails of the Doppler peak which reach even into the low- ℓ region. After the correction, the DMR result becomes $n \approx 1.05 \pm 0.3$ and $Q \approx 17.5^{+3.8}_{-2.8} \mu\text{K}$. Thus our results from a combination of recent CMB measurements in the context of critical density universes agrees well with the DMR-only result and reduces the error bars on both n and Q .

For the standard CDM model of Fig. 8 ($h = 0.50$, $\Omega_o = 1$ and $\Omega_b \approx 0.05$), we obtain $0.90 \leq n \leq 1.17$ (95% CL) and $13 \leq Q \leq 20.5 \mu\text{K}$ (95% CL). Using similar methods and a similar data set, several authors have reported similar results. de Bernardis et al. (1997) find $1.0 \leq n \leq 1.26$ (95% CL). White et al. (1996) find $0.86 < n < 1.10$ (95% CL). Hancock et al. (1997) find $1.0 < n < 1.2$ (68% CL). The variations of these standard model n determinations are probably due to slightly different data sets, different treatments of the Saskatoon calibration and the details of the χ^2 calculation.

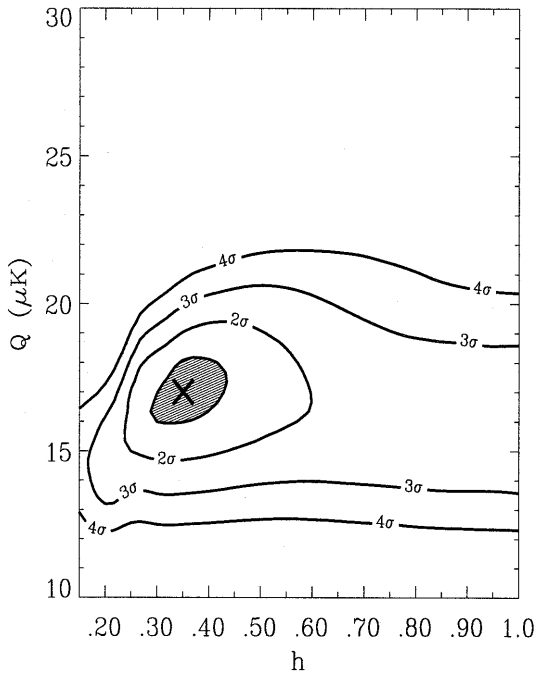


Fig. 6. Likelihood contours in the $h - Q$ plane for $n = 1$ and Ω_b free. $h = 0.35^{+0.08}_{-0.05}$, $Q = 17 \pm 1.0 \mu\text{K}$. Notice that since n has been fixed at 1, the value of Q does not rise in the high h region as it does in the next figure. The 1σ contours are round: there is no correlation between h and Q .

6. Caveats and summary

6.1. Caveats

Our low h measurements are in disagreement with current $z \sim 0$ measurements of the Hubble constant. Possible explanations for this discrepancy could be unidentified systematics in the CMB data or the local h measurements. Galactic foregrounds could be a problem for the CMB while the distance ladder may need some readjusting for the local h measurements (e.g., Feast & Catchpole 1997). The best way to address these problems is with more and better data. This is being done rapidly. New detectors and better designed observations are improving the quality of both the CMB data and the more direct h measurements. SZ and supernovae observations are also increasing the redshift of the h measurements.

A simple answer to the discrepancy between direct h measurements and our results is that the Universe is not well-described by the models considered here. It is possible that one or more of our basic assumptions is wrong, or we could simply be looking at too restricted a region of parameter space. The shape of the primordial power spectrum may be more complicated than the family of models we are using. Inflation may be wrong and structure may not have formed from adiabatic curvature fluctuations. Topological defects may be the origin of structure.

We emphasize that we have only considered a particular type of cosmological scenario, although arguably the simplest; the results we have presented here are valid under the assump-

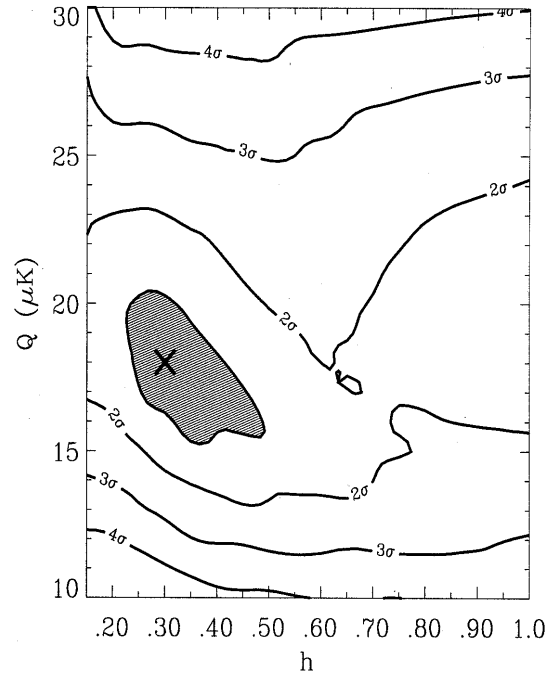


Fig. 7. Likelihood contours in the $h - Q$ plane for n free and Ω_b free. Notice that in the high h region, $Q \sim 20 \mu\text{K}$ is preferred. A comparison with Fig. 5 shows that n and Q are anti-correlated but this is seen more easily in the next two figures.

tion of inflation-based, Gaussian adiabatic initial conditions in a critical density universe ($\Omega_o = 1$) with no cosmological constant. We have not considered any early reionization scenarios or gravitational wave contribution. We have also not included any hot dark matter.

Our $\Omega_o = 1$ assumption can be considered very restrictive since plausible values for Ω_o in the range $[0.2, 1.0]$ can change the power spectrum significantly. For example, the position of the Doppler peak, ℓ_{peak} is roughly proportional to $\Omega_o^{-1/2}$. Thus low Ω_o , by pushing ℓ_{peak} higher may permit higher h values to accommodate the high $\ell_{peak} \sim 270$ of the CMB data. We are in the process of checking this assumption; we consider open models in Lineweaver & Barbosa (1998).

Reionization models can affect the power spectra significantly by lowering the Doppler peak but this can be compensated by n values larger than 1. For example, de Bernardis et al. (1997) have looked at reionization models and find a best-fit early reionization at $z_{reion} \approx 20$ and $n \approx 1.2$.

In paper I we took a brief look at flat- λ models. The supernovae results of Perlmutter et al. (1997) can constrain λ better than the CMB data. The combination of the CMB, BBN and supernovae constraints in flat- λ models yields $0.23 < h < 0.72$.

If gravitational waves or any other effect plays an important role in CMB anisotropy formation, we expect that the inclusion of this effect in the family of models tested, will improve the resulting fits. However the inclusion of gravitational waves seems to make the fits slightly worse without changing the location of the minimum (Liddle et al. 1996b). Bond and Jaffe (1997) analyzed the combined DMR (Bennett et al. 1996), South Pole

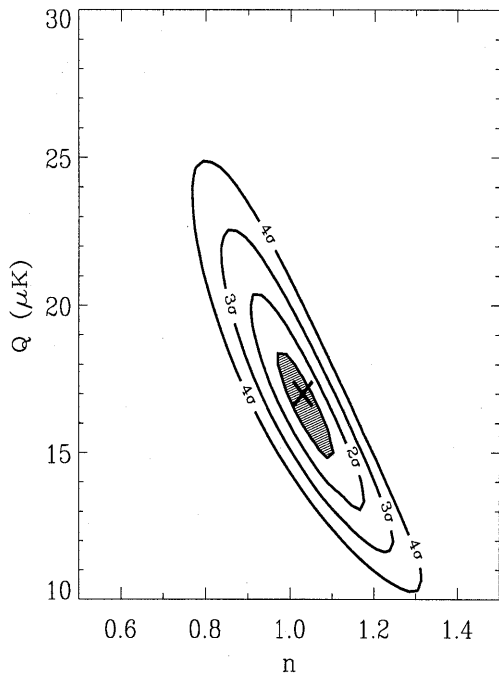


Fig. 8. Likelihood contours in the $n - Q$ plane for $h = 0.50$ and $\Omega_b = 0.05$. Result $n = 1.03^{+0.07}_{-0.06}$ and $Q = 17^{+1.5}_{-2.0}$, or at the 95% CL, $0.90 \leq n \leq 1.17$ and $13 \leq Q \leq 20.5 \mu\text{K}$. This standard model has been looked at by several other workers who obtain similar results (see Sect. 5).

(Gunderson et al. 1995) and Saskatoon (Netterfield et al. 1997) data using signal-to-noise eigenmodes. They looked at the parameters h , n and σ_8 in a variety of models. The inclusion of tensor modes for $n < 1$ models seems to produce small shifts in the likelihood surfaces.

There may be extra-relativistic degrees of freedom (hot dark matter (HDM) or mixed dark matter (MDM)). de Bernardis et al. (1997) found that current CMB anisotropy measurements cannot distinguish between CDM and MDM models. We agree with this assessment and add that HDM and CDM models also cannot usefully be distinguished with current CMB data.

In addition to the h , Ω_b , n and Q considered here, regions of a larger dimensional parameter space deserve further investigation including Ω_o , λ_o , Ω_{HDM} , early reionization parameters such as z_{reion} , tensor mode parameters n_T and T , iso-curvature or adiabatic initial conditions and topological defect models with their additional parameters such as the coherence length. The fact that we obtain acceptable χ^2 values in our small 4-D parameter space lends some support to the idea that we may be close to the right model. However establishing error bars on broad-band power estimates is a relatively new science. If the Universe is not well-described by these models then as the data improve, work like this will show poor χ^2 fits and other regions of parameter space may be preferred.

6.2. Summary

CMB measurements have become sensitive enough to constrain cosmological parameters in a restricted class of models. The

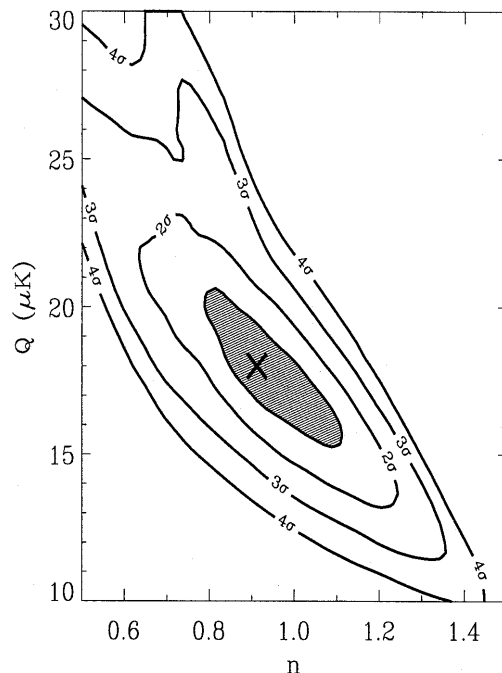


Fig. 9. Likelihood contours in the $n - Q$ plane for h free and Ω_b free. $n = 0.91^{+0.20}_{-0.12}$, $Q = 18 \pm 2.5 \mu\text{K}$. The minimum is at $h = 0.30$, $\Omega_b = 0.07$, and $u = 0.82$.

results we have presented here are valid under the assumption of Gaussian adiabatic initial conditions in a critical density ($\Omega_o = 1$) universe with no cosmological constant. We have explored the 4-dimensional parameter space of h , Ω_b , n and Q . Our CMB-derived constraints on h , Ω_b , n and Q exclude large regions of parameter space. We obtain a low value for Hubble's constant: $H_o = 30^{+18}_{-7}$. The CMB data constrain Ω_b only weakly: $\Omega_b = 0.07^{+0.24}_{-0.07}$. For the slope and normalization of the power spectrum we obtain $n = 0.91^{+0.20}_{-0.12}$ and $Q = 18 \pm 2.5 \mu\text{K}$. The error bars on each parameter are for the case where the other 3 parameters have been marginalized. When we condition on $n = 1$ we obtain the normalization $Q = 17 \pm 1.0 \mu\text{K}$.

CMB constraints are independent of other cosmological tests of these parameters and are thus particularly important. The fact that reasonable χ^2 values are obtained means that the current CMB data are consistent with inflationary-based CDM models with a low Hubble constant. In the context of the models considered, the CMB results are consistent with four other independent cosmological measurements but are in disagreement with more direct measurements of h .

Acknowledgements. The rapidly increasing quality and quantity of data along with the fast Boltzmann code developed by Uros Seljak and Matias Zaldarriaga has made this work possible. We thank Alain Blanchard and Jim Bartlett for useful discussion. We thank Martin White, Douglas Scott and the MAX group for help assembling the required experimental window functions. C.H.L. acknowledges support from the French Ministère des Affaires Étrangères and NSF/NATO post-doctoral fellowship 9552722. D.B. is supported by the Praxis XXI CIENCIA-BD/2790/93 grant attributed by JNICT, Portugal.

References

- Adams, J.A., Ross, G.G., Sarkar, S. 1997, Phys. Rev. B., 391, 271
- Avni, Y. 1976, Ap.J., 210, 642
- Bartlett, J., Blanchard, A., Silk, J., Turner, M.S. 1995, Science, 267, 980
- Bennett, C.L., et al. 1996, Ap.J., 464, L1
- Bersanelli, M., et al. February, 1996, Planck Surveyor (COBRAS/SAMBA) phase A study, ESA Report(D/SCI(96)3)
- Bi, H. & Davidsen A.F. 1997, Ap.J., 479, 523
- Bolte, M. & Hogan, C. 1995, Nature, 376, 399
- Bond, J.R. et al. 1995, Astrophys. Lett. and Comm., 32, 1-6, 53
- Bond, J.R. & Jaffe, A.H., Moriond proceedings, astro-ph/9610091
- Carswell, R.F., Rauch, M., Weymann, R.J., Cooke, A.J. & Webb, J.K. 1994, MNRAS, 268, L1
- Chaboyer, B. 1995, Ap.J. 444, L9
- Cheng, E.S., et al. 1996, Ap.J., 456, L1
- Copi, C.J., Schram, D.N. & Turner, M.S. 1995, Science, 267, 192
- de Bernardis, P. 1997, Ap.J., 480, 1
- Evrard, A.E. 1997, MNRAS, in press, astro-ph/9701148
- Feast, M.W. & Catchpole, R.M. 1997, MNRAS, 286, L1
- Freedman, W.L. 1997, in "Critical Dialogues in Cosmology", ed. N. Turok, in press, astro-ph/9612024
- Gunderson, J.O., et al. 1995, Ap.J., 443, L57
- Hancock, S., et al. 1997, MNRAS, 289, 505
- Jimenez, R., et al. 1996, MNRAS, 282, 926
- Jungman, G., et al. 1996, Phys. Rev. D., 54, 1332
- Kolb, E.W. & Turner, M.S. 1990, "The Early Universe", Addison-Wesley:Redwood City
- Leitch, E., et al. 1997, in preparation
- Liddle A.R. & Lyth D. 1993, Phys. Rep. 231, 1
- Liddle A.R., et al. 1996a, MNRAS, 278, 644
- Liddle A.R., et al. 1996b, MNRAS, 281, 531
- Lineweaver, C.H. 1994, Ph.D. thesis, Berkeley
- Lineweaver, C.H., Barbosa, D., Blanchard, A. & Bartlett, J.G. 1997, A&A 322, 365, astro-ph/9610133
- Lineweaver, C.H., Barbosa, D. 1998, Ap.J. in press, astro-ph/9706077
- Netterfield, C.B., et al. 1997, ApJ, 474, 47
- Oukbir, J., Blanchard, A. & Bartlett, J.G. 1997, A&A, 320, 365
- Peacock, J.A. & Dodds, S.J. 1994, MNRAS, 267, 1020
- Peebles, P.J.E. 1982, Ap.J., 263, L1
- Perlmutter, S., et al. 1997, Ap.J., 483, 565, astro-ph/9608192
- Platt, S.R., et al. 1997, Ap.J., 475, L1
- Press, W.H., Flannery, B.P., Teukolsky, S.A., Vetterling, W.T. 1989, "Numerical Recipes", CUP:Cambridge, p 690
- Rugers, Hogan, C. 1996, Ap.J., 459, L1
- Sarajedimi, A., Lee, Y., Lee, D. 1995, Ap.J., 450, 712
- Salaris, M., Degl'Innocenti, S. & Weiss, A. 1997, Ap.J., 479, 479
- Seljak, U. & Bertschinger, E. 1993, Ap.J., 417, L9
- Seljak, U. & Zaldarriaga, M. 1996, Ap.J., 469, 437
- Smoot, G.F., et al. 1992, Ap.J., 396, L1
- Songaila, A., Cowie, L.L., Hogan, C.J. & Rugers, M. 1994, Nature, 368, 599
- Sugiyama, N. 1995, Ap.J. Sup. Ser., 100, 281
- Tucker, G.S., et al. 1997, Ap.J., 475, L73
- Tytler, D., Fan, X.-M. & Burles, S. 1996, Nature, 381, 207
- Tytler, D. & Burles, S. in "Origin of Matter and Evolution of Galaxies" ed. T. Kajino, Y. Yoshii, S. Kubono (World Scientific:Singapore) in press, 1997, astro-ph/9606110
- Viana, P.T.P. & Liddle, A.R. 1996, MNRAS, 281, 323
- Weinberg, D.H., Miralda-Escudé, J., Hernquist, L. & Katz, N. 1997, Ap.J. 490, in press, astro-ph/9701012
- White, S.D.M., et al. 1993, Nature, 366, 429
- White, M., Viana, P.T.P., Liddle, A.R., Scott, D. 1996, MNRAS, 283, 107
- Wright, E.L., Hinshaw, G. & Bennett, C.L. 1996, Ap.J., 458, L53
- Wright, E.L., 1995, Proc. of the CWRU COBE meeting, astro-ph/9408003
- Zaldarriaga, M., Spergel, D.N. & Seljak, U. 1997, astro-ph/9702157